

**Multivariate Analysis of Factors Regulating the Formation of Synthetic
Allophane and Imogolite Nanoparticles**

McNeill John Bauer

Thesis submitted to the faculty of the Virginia Polytechnic Institute and
State University in partial fulfillment of the requirements for the degree of

Master of Science
In
Geosciences

Frederick M. Michel, Chair
Feng Lin
Clément Levard

August 1, 2019
Blacksburg, Virginia

Keywords: Imogolite, allophane, synthesis, modeling, growth

Multivariate Analysis of Factors Regulating the Formation of Synthetic Allophane and Imogolite Nanoparticles

McNeill John Bauer

Abstract

Imogolite and allophane are nanosized aluminosilicates with high value in industrial and technological applications, however it remains unclear what factors control their formation and abundance in nature and in the lab. This work investigated the complex system of physical and chemical conditions that influence the formation of these nanominerals. Samples were synthesized and analyzed by powder x-ray diffraction, *in situ* and *ex situ* small angle x-ray scattering, and high-resolution transmission electron microscopy. Multivariate regression analysis combined with linear combination fitting of pXRD patterns was used to model the influence of different synthesis conditions including concentration, hydrolysis ratio and rate, and Al:Si elemental ratio on the particle size of the initial precipitate and on the phase abundances of the final products. The developed models described how increasing Al:Si ratio, particle size, and hydrolysis ratio increased the proportion of imogolite produced, while increasing the concentration of starting reagents decreased the final proportion. The model confidences were >99%, and explained 86 to 98% of the data variance. It was determined from the models that hydrolysis ratio was the strongest control on the final phase composition. The models also were able to consistently predict experimentally derived results from other studies. These results demonstrated the ability to use this approach to understand complex geochemical systems with competing influences, as well as provided insight into the formation of imogolite and allophane.

Multivariate Analysis of Factors Regulating the Formation of Synthetic Allophane and Imogolite Nanoparticles

McNeill John Bauer

General Audience Abstract

Allophane and imogolite are nanosized aluminosilicate minerals and strongly control the physical and chemical behavior of soil. They hold promise for use in technological applications. In nature, allophane and imogolite are often observed together in varying proportions. Similarly, laboratory synthesis by various methods usually does not result in pure phases. These observations suggest they form at the same time, at a wide range of solution chemical conditions. It remains unclear what factors determine how and when these phases form in solution, which limits our understanding of their occurrence in nature and the laboratory. The objective of this study is to understand and explain what solution chemical and physical conditions control the formation of synthetic imogolite and allophane. We did this by utilizing a unique approach where we systematically varied starting conditions of formation of these particles, and then used analytic and statistical methods to develop a model that describes the relationship between each of the starting conditions – concentration, size, pH, atomic ratios, and hydrolysis ratios, and how those effect the phase abundance of the particles.

Acknowledgements

I would like to thank Marc Michel for guiding me through this process and helping support and shape my scientific mind. I would further like to thank my proxy committee members Nancy Ross and Feng Lin who stepped in to help out at the last minute and provided valuable feedback and a helpful outsider perspective on the project. I would like to thank Clement Levard as well as Don Rimstidt who provided direction and purpose to the project. I would also like to thank my research group, Aly, Allie, Ali, and Rui for welcoming me in and being great mentors and friends. I want to additionally thank Allie who took TEM images and did EDS analysis for me. I would like to thank IGEP and NSF for funding my assistantship and the project, respectively. I would like to acknowledge NanoEarth as well as Virginia Tech Geosciences for fostering a positive environment to work. Finally I would like to thank family and friends who supported me throughout this work.

Table Of Contents

Abstract.....	ii
General Audience Abstract.....	iii
Acknowledgements.....	iv
List of Figures.....	vi
List of Tables.....	vii
1. Introduction.....	1
2. Methods.....	3
2.1 Synthesis.....	3
2.2 Powder X-Ray Diffraction analysis.....	3
2.3 Small Angle X-Ray Scattering.....	3
2.4 Transmission Electron Microscopy.....	4
2.5 Multivariate Linear Regression Analysis.....	4
2.6 Statistical interpretation.....	4
3. Results.....	5
3.1 Syntheses of nanosized aluminosilicate.....	5
3.2 Phase identification.....	6
3.3 Linear combination fitting.....	7
3.4 Multivariate regression modeling of data set 1.....	8
3.5 In situ Dv(R) particle size data.....	11
3.6 Multivariate regression modeling of data set 2.....	12
4. Discussion.....	15
4.1 Growth stages of aluminosilicate nanoparticles.....	16
4.2 Influence of synthesis conditions on phase abundance.....	16
4.3 Evidence of allophane versus proto-imogolite production in the literature..	17
4.4 Modeled versus experimental pXRD patterns produced in literature.....	17
4.5 The significance of the in situ data.....	19
4.6 Multivariate approach to explaining geochemical systems.....	19
5. Conclusions.....	20
Works Cited.....	21

List of Figures

Figure 1. Example of pH change observed during the first hour of synthesis.....	5
Figure 2. pXRD and HR-TEM analyses of the different endmembers used for LCF analysis.....	7
Figure 3. Measured versus modeled result of imogolite proportion of synthesis products.....	9
Figure 4. Measured versus predicted result of proto-imogolite proportion of synthesis products.....	10
Figure 5. Measured versus predicted result of amorphous silica proportion of synthesis products.....	11
Figure 6. A representative data set given showing the quality of the SAXS sample....	12
Figure 7. Residuals of the imogolite proportion models for the data without and with particle size data collected.....	14
Figure 8. Residuals of the proto-imogolite proportion models for the data without and with particle size data collected.....	15
Figure 9. Experimental XRD pattern of Ohashi et al. reported synthetic allophane, and Du at al. reported synthetic imogolite.....	18

List of Tables

Table 1. Synthesis starting condition and normalized LCF phase abundances.....	8
Table 2. Data outlining the second set of syntheses, with starting conditions of synthesis products, and the resulting phase abundance, with the addition of Dv(R) particle size data.....	13

1. Introduction

Nanosized aluminosilicates strongly control soil physical properties and affect soil and water quality by controlling the transport and fate of nutrients and environmental contaminants. They have significant potential in industrial and technological applications (Paineau et al., 2018; Thill, 2016; Maillet et al., 2011; Iyoda et al., 2014) and are also thought to be the precursors to hydrous smectite and other more crystalline clay minerals (Harsh, 2002). Of the nanosized aluminosilicates observed in natural soils, imogolite ($\text{Al}_2(\text{OH})_3\text{SiO}_3\text{OH}$) and allophane ($\text{Al}_2\text{O}_3 \cdot (\text{SiO}_2)_{1.3-2} \cdot (2.5-3)\text{H}_2\text{O}$) are the most abundant (Parfitt, 2009) and typically occur together in varying proportions (Harsh, 2002). Despite the importance of natural and synthetic imogolite and allophane it remains unclear how physical and chemical conditions during formation control their abundance. This limits our ability to explain their distributions and impacts in natural soils, as well as the potential to synthesize pure phases with controlled properties for use in technological applications.

The primary distinguishing factor between imogolite and allophane is their morphologies (Abidin et al., 2007). Imogolite forms as nanotubes 2-3 nm in diameter and with lengths extending for 100's of nm to μm (Ohashi et al., 2002; Gustafsson, 2001). Allophane is most often described as a pseudo-spherical nanoparticle 3-5 nm in diameter with a hollow interior, although direct images of well-formed allophane nanospheres remain scarce (Sharp and Chang, 2017). Further, the 3-dimensionality of the particles has been questioned by some researchers, who suggest that TEM imaging cannot definitively differentiate a sphere from a 2-D structure (Levard et al., 2012; Hemni and Wada, 1976). For this reason, some have argued that what is often identified as allophane may in fact be only roof tile-shaped fragments of imogolite. These have been referred to as "proto-imogolite" based on evidence indicating that in solution, they eventually transform to imogolite (Levard et al., 2010). Both are composed of a common local structure comprised of gibbsite-like sheets of aluminum hydroxide ($\text{Al}(\text{OH})_3$). On one side of the sheet, isolated silica (SiO_4) tetrahedra occupy the center position of the six-membered rings formed by the Al octahedra (Levard et al., 2012). The curvature of the particles is thought to arise from strain caused by the differences in size of the silica tetrahedra versus the aluminum octahedra (Thill et al., 2017).

The morphological difference between imogolite and allophane is driven by the degree of curvature in the precursor particles, where one and two directions of curvature form tubes and spheres respectively. What determines this critical parameter remains unclear. Previous experimental studies of imogolite and allophane formation have tested separately the effects of starting concentration, pH, and elemental ratios on the two different morphologies (Wang et al., 2018; Ohashi et al., 2002; Montarges-Pelletier et al., 2005; Du et al., 2018). A study based on numerical modeling suggested that there is a critical size to the proto-imogolite particles previously described (Thill et al., 2017). It predicts that particles larger than 4 nm favor imogolite formation whereas smaller particles result in allophane. Others have suggested that excess silica to aluminum in the starting solution will suppress imogolite formation due to the limited capacity for silica polymers in the inner tube. Excess silica may be accommodated by

silica polymers residing in the larger interiors of spherical allophane and/or by the increased number of reactive surface sites on proto-imogolite fragments (Levard et al., 2012). Another study suggested that imogolite is not favored at hydrolysis ratios less than 1.5 due to differences in imogolite and allophane stabilities at different pH and OH:Al ranges (Levard et al., 2011a). Taken together these prior studies suggest that imogolite and allophane formation may be influenced by two or more competing factors.

This paper explains how key variables including concentration, elemental Al:Si ratio, hydrolysis ratio and speed, and precursor particle size impact the formation of imogolite. Systematic synthesis experiments were combined with *in situ* and *ex situ* analytical characterization and multivariate linear regression analysis to determine the quantitative influence each factor had on final phase abundance. We found no evidence for well-formed allophane nanospheres at any of our synthesis conditions. Instead, only imogolite nanotubes and what we interpret as proto-imogolite, which has physical characteristics similar to what has been described previously by Levard et al. (2010). This is the first study designed to unravel the competing effects of these different synthesis variables, as well as to factor in the role of precursor particle size on imogolite formation. The results are important for greater understanding of aluminosilicate synthesis, where individual variables can be isolated and understood for their effect on the system. The framework of the study can be adapted and utilized for other geochemical processes where competing effects complicate the study of the system.

2. Methods

2.1 Synthesis:

Nanosized aluminosilicates were synthesized at room temperature using a method adapted from the literature (Iyoda et al., 2014; Montarges-Pelletier et al., 2005; Wada et al., 1979; Huang et al., 2016). Aluminum chloride hexahydrate ($\text{AlCl}_3 \cdot 6\text{H}_2\text{O}$, Sigma-Aldrich, 99%) was mixed with 50 mL of 18.2 M Ω -cm ultrapure water in a standard borosilicate glass reactor to reach concentrations ranging from 0.005 M to 0.2 M. Tetraethyl orthosilicate (TEOS, Sigma-Aldrich, 99.9%) was immediately added to reach Al:Si molar ratios ranging from 0.5 to 2. TEOS was added prior to inducing hydrolysis to minimize silica polymerization. Hydrolysis was achieved by pumping a 0.1 M sodium hydroxide solution (NaOH, Fisher Scientific, 99%) at rates ranging from 0.2 to 10 mL min⁻¹, using a peristaltic pump (Ismatec IPC8) fitting with Tygon 2-stop tubing (Ismatec SC0824) to achieve [OH]:[Al] hydrolysis ratios of 1 to 3. The resulting solution was stirred at 400 RPM for 1 hour, while monitoring pH at 5-second intervals (Oakton PC 2700). The solutions were then transferred into 250 mL anaerobic glass bottles with butyl rubber stoppers and aluminum seals (Chemglass Life Sciences CLS-4217-03), and then heated constantly at 95°C for 7 days (Fisher Isotemp 215G). The final solution was then dialyzed against 18.2 M Ω -cm ultrapure water using a 12-14,000 Da, 25mm diameter standard grade membrane (Spectra Por) for 2 weeks, until the conductivity of the solution reached below 2 μS . The dialyzed solution was then dried at 40°C to obtain a white powder for further analysis. Synthesis of an amorphous silica sample used as a reference was reported previously [Cismasu et al., 2014]

2.2 Powder X-ray diffraction analysis:

Powder x-ray diffraction (pXRD) data were collected using a Rigaku MiniFlex II Desktop x-ray diffractometer equipped with a $\text{CuK}\alpha$ source (30 kV to 15 mA). Dried samples were homogenized using an agate mortar and pestle and the powders were pack mounted into a well in a zero background single crystal silicon holder. Diffracted intensities from the samples were collected from 5 to 80° 2 θ in 0.01° increments. Exposure time was 2 seconds per step and the sample holder was rotated continuously during data collection. Linear combination fitting (LCF, WinXAS 3.0) was used to estimate the proportions of imogolite, proto-imogolite, and amorphous silica in each synthesized product. pXRD patterns of imogolite, proto-imogolite, and amorphous silica were selected as endmember components based on maximum purity assessed by pXRD comparisons, SAXS, and TEM data (see Section 3.2). Ternary combinations of the endmember pXRD patterns were fitted to each sample pattern and weight fractions for each component were determined using a least-squares minimization procedure. The sum of the weight fractions was normalized to 1.0. Residuals were visually assessed.

2.3 Small Angle X-ray Scattering:

Small angle x-ray scattering (SAXS) data were collected using a Panalytical Empyrean Nano Edition multi-purpose x-ray scattering platform equipped with a Cu anode ($\lambda_{Cu_{K\alpha}} = 1.5406 \text{ \AA}$) and elliptic beam focusing optic with a $1/32^\circ$ fixed slit. Diffracted intensities from the samples and backgrounds were collected from -0.15 to $6^\circ 2\theta$ in approximately 0.014° increments using a GaliPIX^{3D} area detector or proportional detector. Exposure times ranged from 60-320 sec/point. Dry samples were flat mounted between Mylar films and measured in a ScatterX⁷⁸ evacuated sample holder and beam path. *In situ* experiments were performed using a custom liquid flow cell designed for use with the ScatterX78 vacuum stage. In brief, the synthesis solution was pumped continuously from the reactor into the flow cell and then returned to the reactor using a peristaltic pump. Scans were collected continuously during each experiment to monitor for changes in particle size distribution during initial hydrolysis and subsequent mixing. Once the solution began to show stable results, usually up to 90 minutes into the experiment, the final 5 scans were averaged and the background subtracted. Volume-weighted size distribution (Dv(R)) analysis (see Glatter, 1980) were performed using EasySAXS (Panalytical).

2.4 Transmission Electron Microscopy:

High-resolution transmission electron microscopy (HR-TEM) imaging was performed on a JEOL 2100 operating at 200 KeV (NCFL, ICTAS, Virginia Tech). Samples were diluted to 10 ppm, and then dialyzed against methanol using a 12-14,000 Da, 25mm diameter standard grade membrane (Spectra Por). Before imaging, samples were placed in a sonicating bath for 1 minute to disperse aggregates. The samples were mounted on Lacey-carbon, 300 mesh, copper-backed grids from Ted Pella. The grids were dried in air and stored in a benchtop vacuum chamber.

2.5 Multivariate Linear Regression Analysis:

Multivariate linear regression analysis was applied to LCF data that estimated each endmember proportion of imogolite, proto-imogolite, and amorphous silica. The starting physical and chemical conditions were analyzed using multivariate regression with respect to the final phase composition of the synthesized products.

In the case where a dependent variable Y can be described by a relationship to some number of independent variables x_i by some function $Y=f(x_i)$, multivariate regression analyses can be employed to determine the exact nature of the relationship of each independent variable to the dependent variable, while simultaneously controlling for all of the other independent variables. (Mansouri et al., 2018). This analysis was performed using the R software, RStudio.

2.6 Statistical interpretation

When analyzing the effectiveness of the multivariate models, R^2 represents of how much of the variance in the data is explained in the model. Because each independent variable consequently increases the R^2 value, an adjusted R^2 calculation must be performed. This accounts for the increase in R^2 with additional variables, and gives a true representation of how much of the data is explained by the model.

The root mean square error (RMSE) is the standard deviation of the residual of the data. It gives an estimation of predictive power of the model.

Durbin and Watson (DW) statistics were used to test for autocorrelation in the residuals from the regression analysis (Durbin and Watson 1950, 1951). Random residuals are a crucial component of a predictive model, correlation in the residuals indicates some predictive information is not described by the model. The DW statistic (d) always lies between 0 and 4. The null hypothesis is confirmed when d lies between 1.5 and 2.5, while higher and lower values suggest autocorrelation.

3. Results

3.1 Syntheses of nanosized aluminosilicates

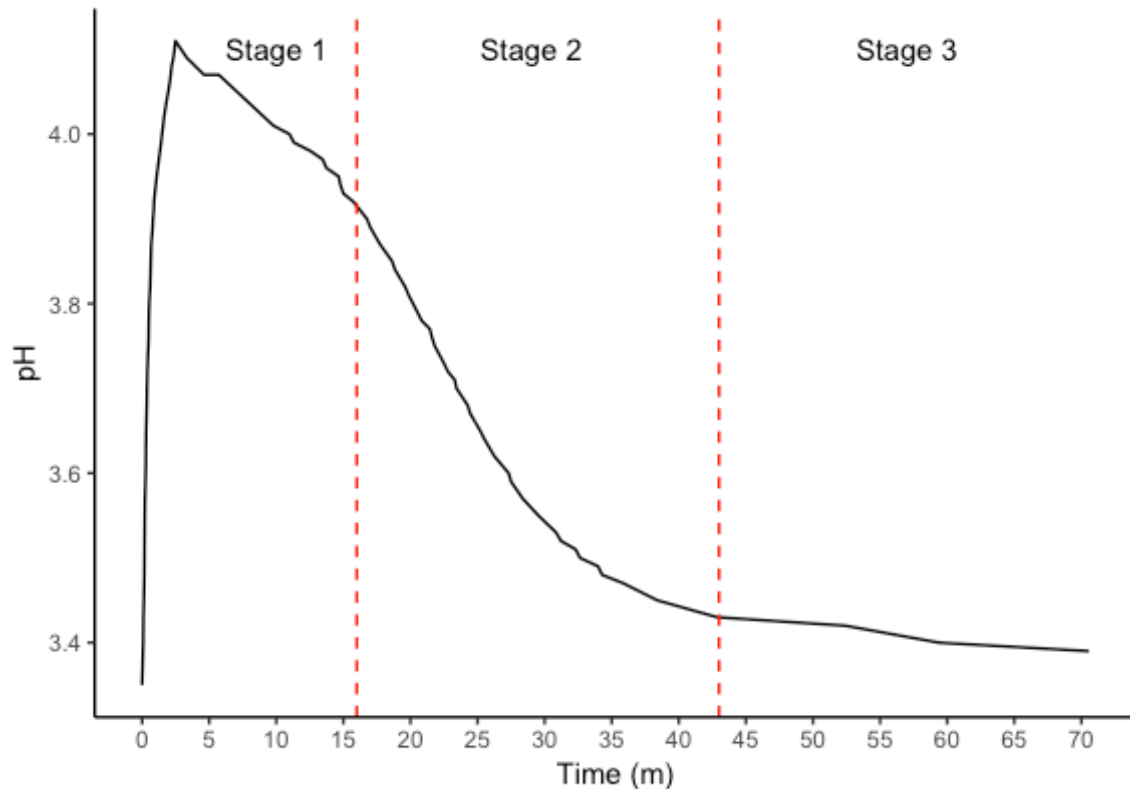


Figure 1 Example of pH change observed during the first hour of synthesis, broken into three growth stages. This synthesis was performed using 0.05M $AlCl_3$ with a 1:2 Al:Si

ratio, and a 1:1 OH:Al ratio. Time point zero corresponds with the starting pH and the beginning of NaOH addition.

A pH and visual study of the synthesis process suggested three distinct growth phases as displayed in Figure 1. NaOH addition during the initial minutes of the experiment (Stage 1) results in a rapid rise in pH. The pH begins to decrease as soon as NaOH addition is finished, which is approximately at the maximum between 0-5 min. During this period a translucent gel-like phase appears in the solution. Stage 2 is marked by a period of rapid pH decrease where the solution, depending on starting conditions, either returns to clear or develops a white cloudy precipitate, which persists for the rest of the synthesis. Stage 3 is the period in which the pH becomes approximately stable. The solution was then placed in anaerobic bottles and heated for 7 days at 95C, after which a cloudy white precipitate would often form. When dried, the solution would produce a fine white powder.

3.2 Phase identification

The final solids of each synthesis were characterized by HR-TEM imaging and/or pXRD analysis. Three distinct phases were identified. Figure 2 presents pXRD profiles for samples consisting of pure imogolite and proto-imogolite, as well as for an amorphous silica reference. HR-TEM images of imogolite and proto-imogolite are also given in Figure 2, along with an example of amorphous silica observed in one of the synthesis products. All three pXRD profiles show a series of one or more broad, weak peaks consistent with materials lacking long-range periodicity (i.e., short-range ordered). The pXRD patterns of each agree with previously reported spectra (Arancibia-Miranda et al., 2013; Levard et al., 2012; Musić et al., 2011). HR-TEM images of the imogolite and proto-imogolite endmembers generally showed highly aggregated nanoparticles with different morphologies (Figure 2A and B). The imogolite sample exhibited fairly distinct and elongated nanotube-like shapes. The sample that was expected to be allophane based on its pXRD characteristics showed no evidence of well-formed spherical nanoparticles. Thus, we assumed that the morphological characteristics of this sample were consistent with proto-imogolite. Amorphous silica consisted of aggregates of globular with varying particle sizes in the range of 10's to 100's of nms (Figure 2C). This was confirmed through EDS analysis which showed the sample contained only silicon (need to add this to methods now but not sure on specs yet). Overall, the sizes and morphologies observed in HR-TEM were generally consistent with what has been reported previously for synthetic imogolite, proto-imogolite, and amorphous silica.

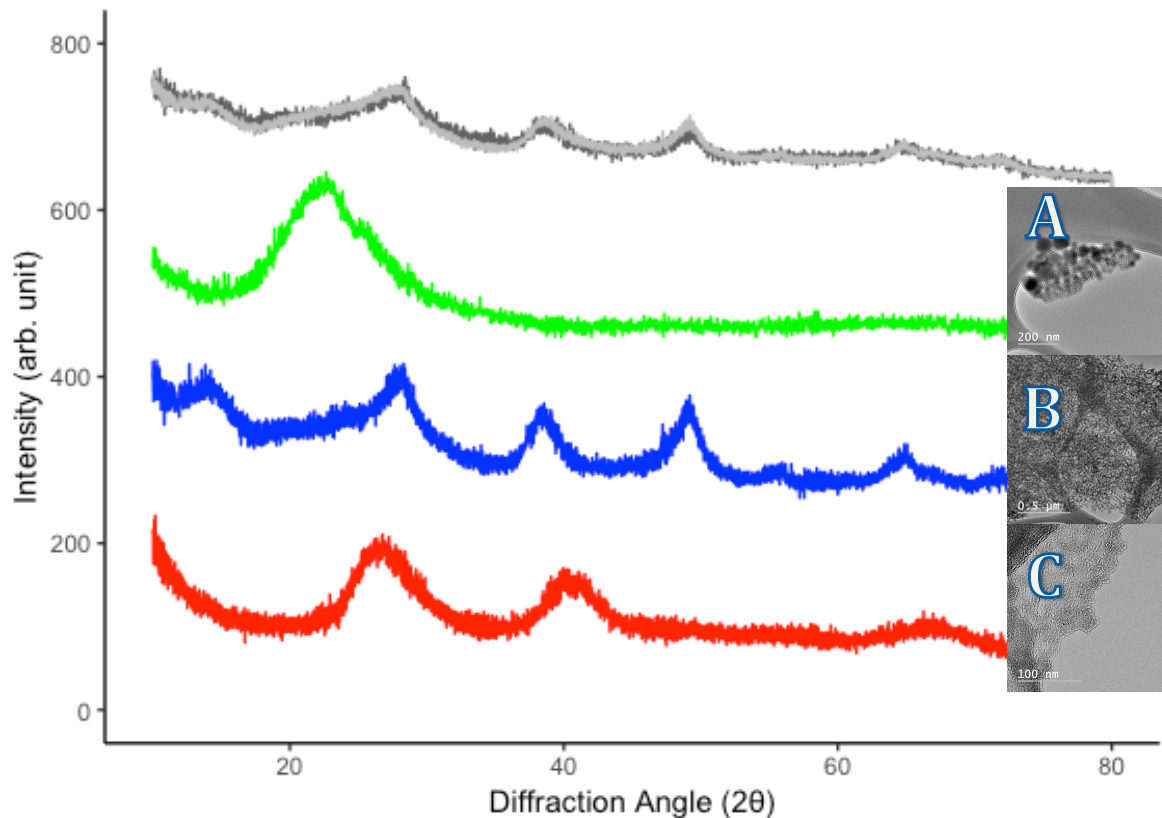


Figure 2 pXRD and HR-TEM analyses of the different endmembers used for LCF analysis. Representative TEM images of A) amorphous silica B) imogolite and C) proto-imogolite endmembers. It also includes a synthesized product shown in dark grey, and the resulting LCF fit in light gray.

The majority of the other products of the different synthesis experiments did not result in a pure single phase as commonly found in natural samples, (Harsh, 2002), but instead contained a mixture of the three different endmembers. Qualitative evidence for these mixtures was provided by pXRD, which showed combinations of distinct pXRD peaks for imogolite, proto-imogolite and/or amorphous silica all present in a single sample (Table 1).

3.3 Linear combination fitting

Linear combination fitting of pXRD was used to quantify the abundances of imogolite, proto-imogolite, and amorphous silica in a set of 23 synthesis products. An example of the LCF fit of a pXRD pattern from a synthesized product is shown in figure 2. Table 1 shows the results of LCF analysis and summarizes the starting conditions used for each synthesis. LCF results show that the abundances of proto-imogolite and imogolite varied from approximately 0 up to 100% for the different synthesis conditions. The abundance of amorphous silica, which has been reported previously in studies of imogolite and proto-imogolite synthesis (Wada et al., 1979), varied between

approximately 0 up to 31%. The data illustrate how variations in the abundances of proto-imogolite, imogolite, and amorphous silica occur with differences in synthesis conditions.

Table 1
Synthesis starting condition and normalized LCF phase abundances

Concentration (M)	Hydrolysis Ratio	NaOH addition (ml/min)	Al:Si Ratio	Proto-imogolite Proportion	Imogolite Proportion	Amorphous Silica Proportion
0.15	3.00	10.00	1.50	0.00	1.00	0,00
0.13	3.00	10.00	1.50	0.00	1.00	0.00
0.13	1.00	2.00	1.50	0.66	0.12	0.22
0.10	3.00	10.00	1.50	0.05	0.95	0.00
0.18	1.00	2.00	1.50	0.64	0.12	0.24
0.13	1.00	2.00	1.00	0.75	0.29	0.00
0.15	1.00	2.00	1.00	0.73	0.10	0.17
0.01	3.00	2.00	1.50	0.00	1.00	0.00
0.02	1.00	10.00	1.50	0.48	0.33	0.19
0.15	3.00	10.00	1.50	0.00	0.78	0.23
0.18	3.00	10.00	1.50	0.32	0.49	0.19
0.18	1.00	2.00	1.50	0.62	0.08	0.29
0.18	3.00	10.00	1.50	0.62	0.24	0.14
0.18	1.00	2.00	1.00	0.29	0.15	0.56
0.20	1.00	2.00	2.00	0.74	0.00	0.27
0.18	1.00	2.00	2.00	0.79	0.00	0.24
0.13	1.00	10.00	2.00	0.53	0.14	0.34
0.19	1.00	2.00	1.00	0.62	0.03	0.35
0.19	1.00	2.00	2.00	0.48	0.06	0.46
0.16	1.00	10.00	1.50	0.58	0.13	0.29
0.16	1.00	10.00	1.00	0.58	0.01	0.40
0.16	1.00	2.00	2.00	0.60	0.20	0.20
0.20	1.00	10.00	1.50	1.00	0.00	0.00

3.4 Multivariate regression modeling of data set 1

The data in Table 1 was analyzed using multivariate regression, which produced a model of imogolite proportion that followed the following relationships: $I = 0.009 + 0.35hydro - 1.82c + 0.11Al : Si$ [Eq. 1]. The model was used to produce data of predicted imogolite proportion, which was compared to the experimentally determined proportions in Figure 3.

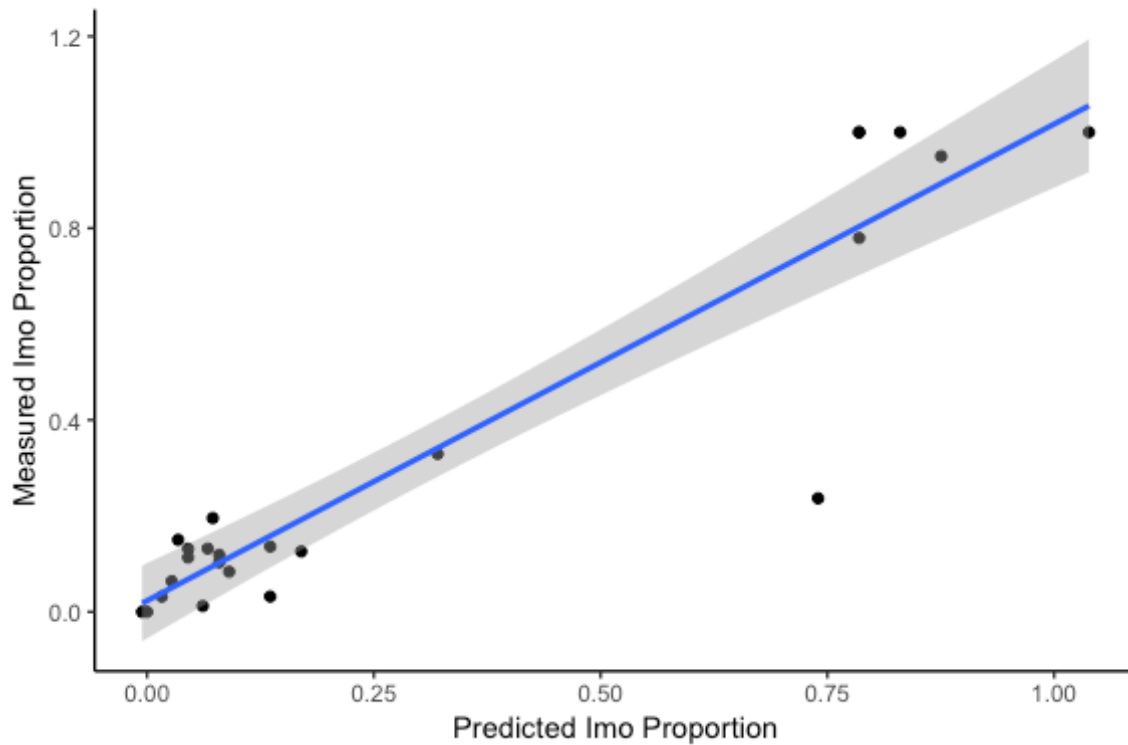


Figure 3
Measured versus modeled result of imogolite proportion of synthesis products

The model demonstrates that imogolite proportion increases with increasing hydrolysis ratio and Al:Si ratio, and that the proportion of imogolite decreases as concentration of starting reagents increases. The model was found to be significant, with a p-value of 1.3×10^{-9} , and an R^2 of 0.86, which means that the model explains 86% of the variance in the data. The starting concentration and hydrolysis ratio factors were both statistically significant, with >99.99% and >99% confidence respectively. Both the intercept and elemental ratio factor both failed a 0.05 p value significance test.

The RMSE is 0.13, meaning the model can predict the imogolite proportion to within $\pm 13\%$. The DW statistic for the residuals of this model is 2.26, which with a 99% confidence rate the null hypothesis can be rejected, suggesting there is no autocorrelation in the residuals.

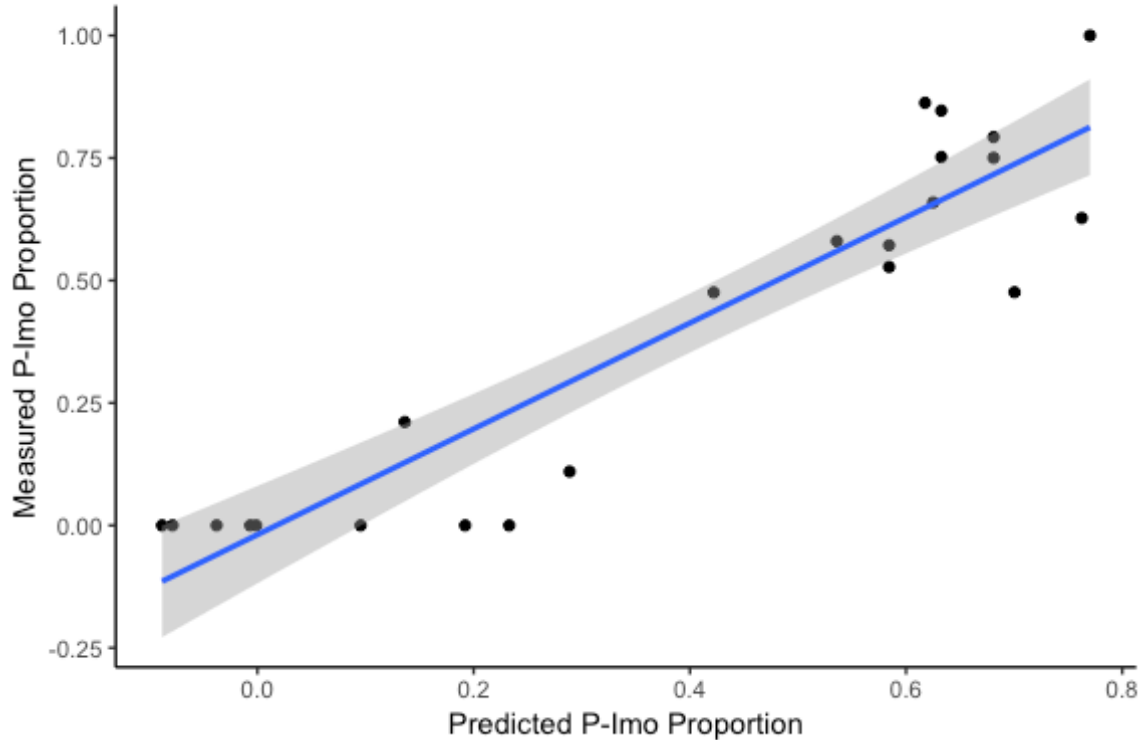


Figure 4

Measured versus predicted result of proto-imogolite proportion of synthesis products

A model for determining the proto-imogolite proportion was also developed, and is described as follows: $PI = 1.01 - 0.30hydro + 0.93C - 0.092Al : Si$ [Eq. 2]

The model describes that as concentration of starting reagents increases, the proportion of proto-imogolite in final the product also increases. It also suggests that as the hydrolysis ratio and elemental ratio increase the proto-imogolite proportion is decreased, directly opposed to the imogolite relationships.

This model was found to be significant, with a p-value of 1.62×10^{-9} . It has an R^2 of 0.88; the model does not explain 12% of the variance of the data. The intercept and hydrolysis ratio factor were found to be significant with a >99.99% confidence. The concentration factor was also found to be significant to a p value of 0.05. As with the other model, the elemental ratio was insignificant, with a p-value of 0.22. The RMSE is similar to the imogolite model, but slightly lower at 0.12. The DW statistic was found to be 0.5, which rejects the null hypothesis and suggests positive autocorrelation in the residuals, meaning there is some predictive measure in the data that is not captured by the model.

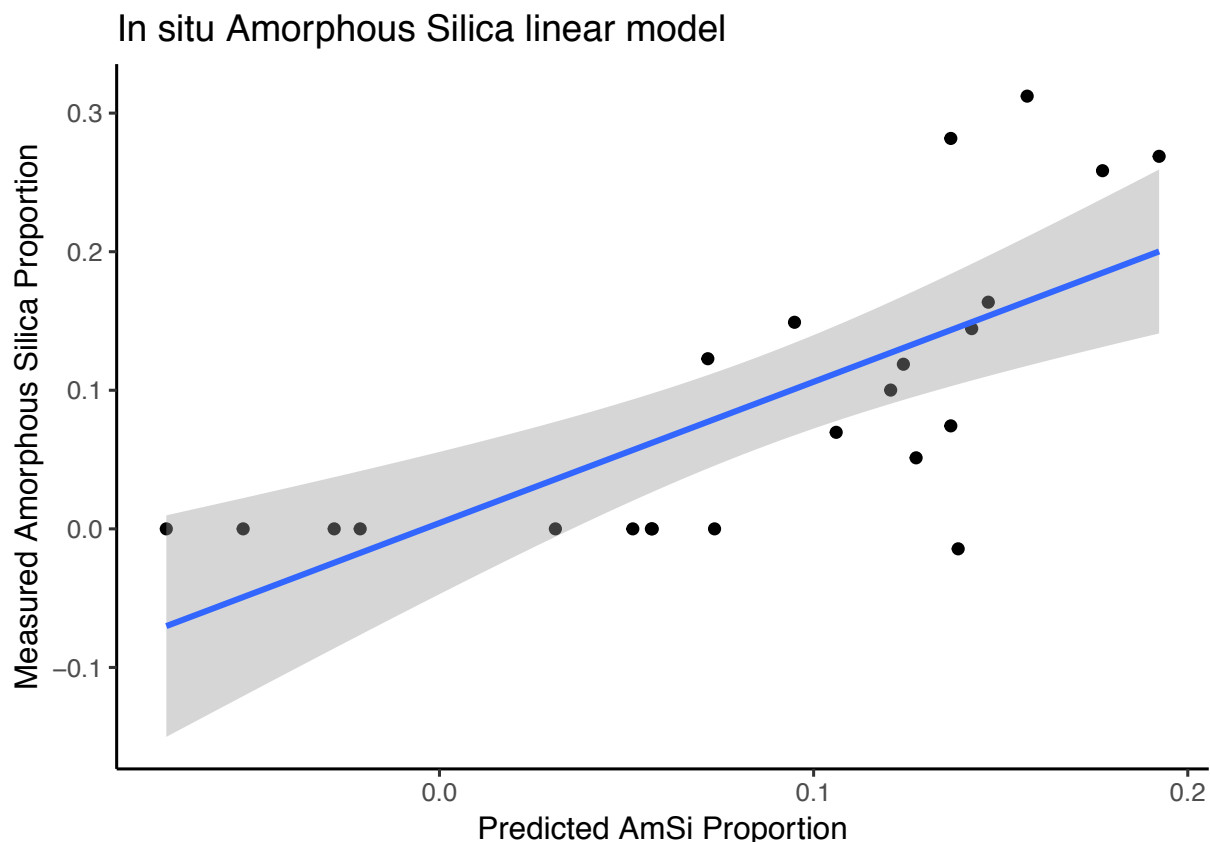


Figure 5

Measured versus predicted result of amorphous silica proportion of synthesis products

Amorphous silica was found to have significant variance and limited predictive power, and so a full model is not reported. The model is, based on p-values, 9 orders of magnitude less significant than the proto-imogolite and imogolite models. The overall significance is 99%, but the average confidence of all of the individual factors is 65%. None of the variables were found to be significant. Intuitively however, the Al: Si ratio suggested that as Si increases relative to Al, total amorphous silica proportion increases at 85% confidence. The p-value of the model is 0.01, but the R^2 value is 0.32, meaning the model explains only 32% of the variance of the amorphous silica proportion. The DW statistic for the residuals is 0.68, indicating positive autocorrelation.

3.5 *In situ* $D_v(R)$ particle size data

We performed *in situ* SAXS studies where we repeated the outlined synthesis procedures and measured average and median particle size (Figure 6). We have confirmed that increasing concentrations of starting reagents reduces the average precursor particle size, following equation : $R_{avg} = 2.3 - 9.6C - 0.88s + 0.68H - 0.33Al : Si$ [Eq. 3]

This model explains average precursor particle size where C is starting concentration of reagents, s is speed of NaOH addition, H is hydrolysis ratio, and Al:Si is elemental ratio. The model explained 91% of the variance in the data, with a confidence >99.99%, and had random residuals as evidenced by a DW statistic of 2.08. Increasing concentration decreases average precursor particle size, and has the largest influence on the final size distribution of the particles.

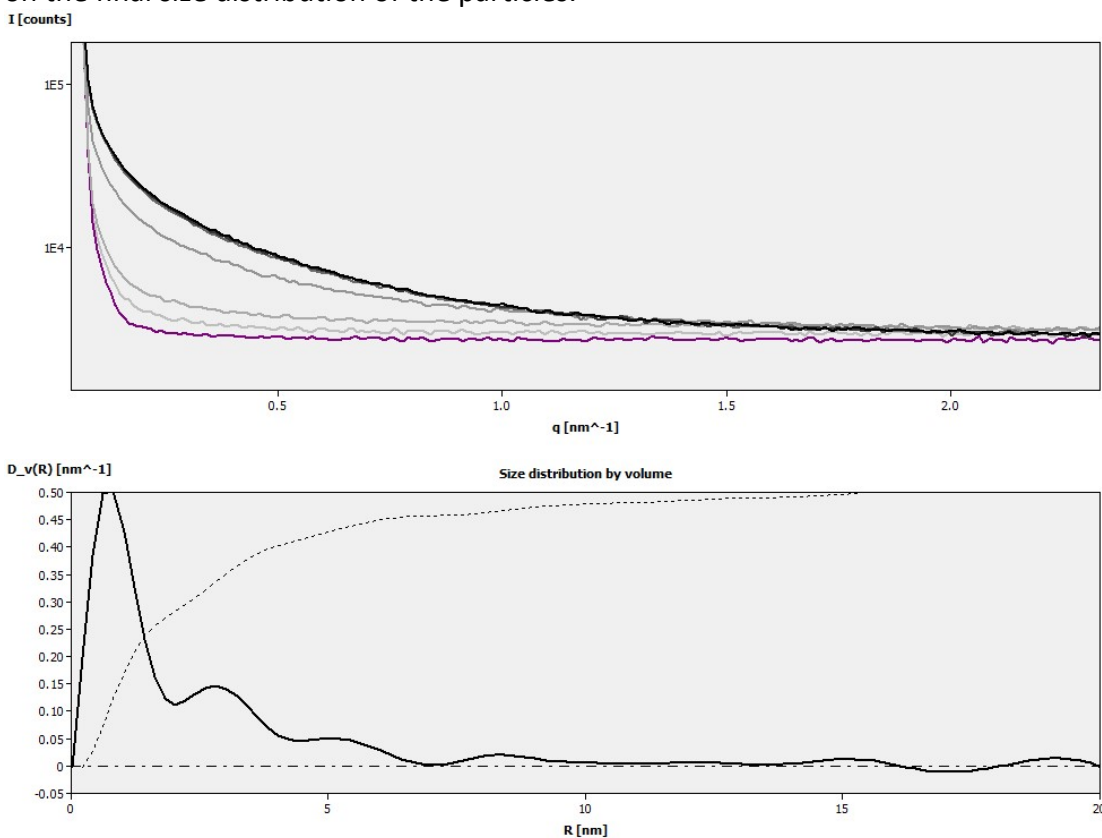


Figure 6. A representative data set given showing the quality of the SAXS sample (Grey to black), background (Purple) (Top), as well as the DvR fit, over a time series of data collected (Bottom)

Tracking $D_v(R)$ results *in situ* through the first hour of synthesis yielded similar results to the pH study shown in Figure 1, and is shown in Figure 6. Three stages emerged again, where stage 1 shows rapid growth and nucleation of particles, with increasing average particle size. Stage 2 shows minimal growth in particle size but continued nucleation, and by stage 3 the $D_v(R)$ analysis shows no growth over time in size or significant nucleation of particles

3.6 Multivariate regression modeling of data set 2

A second set of syntheses was performed *in situ*, and using $D_v(R)$ analysis average and most frequent particle size data were added to the system. These experiments aimed to quantify the sizes of the particles that would be heated and

aged to obtain the final synthesis products. Once stage 3 was reached, and there was no longer evidence of nucleation or growth, the particle size data was recorded, and added to the set of synthesis conditions (table 2). The data was then analyzed identically to the previous data set to produce proportion abundance models. The imogolite proportion was modeled as follows:

$$I = -0.046 + 0.34hydro - 0.40C - 0.073Al : Si + 0.11R_{avg} - 0.38R_{med} \text{ [eq. 4]}$$

Table 2 Data outlining the second set of syntheses, with starting conditions of synthesis products, and the resulting phase abundance, with the addition of Dv(R) particle size data

Concentration (M)	Hydrolysis Ratio	NaOH addition (ml/min)	Al:Si Ratio	Mean Radius (nm)	Median Radius (nm)	Proto-imogolite Proportion	Imogolite Proportion	Amorphous Silica Proportion
0.1	1	5	1	0.73	0.70	0.86	0.15	0.00
0.1	1	2	1	0.80	0.75	0.82	0.12	0.05
0.15	1	1	2	0.93	0.70	0.75	0.25	0.00
0.15	1	5	2	0.57	0.56	0.79	0.21	0.00
0.15	1	0.5	2	0.87	0.90	0.85	0.08	0.07
0.15	1	2	2	0.78	0.80	0.71	0.19	0.10
0.1	1	0.5	2	0.90	0.90	0.58	0.26	0.16
0.175	1	5	2	0.75	0.80	0.81	0.11	0.07
0.175	1	2	2	0.82	0.80	0.63	0.23	0.14
0.175	1	5	1	0.66	0.60	0.63	0.11	0.26
0.15	1	5	1	0.79	0.75	0.57	0.12	0.31
0.175	1	0.5	2	0.82	0.80	0.56	0.15	0.28
0.125	1	1	2	0.91	0.90	0.85	0.03	0.12
0.175	1	0.5	1	0.84	0.75	0.64	0.10	0.27
0.125	1	5	2	0.73	0.70	0.57	0.31	0.12
0.125	1	2	2	0.85	0.80	0.63	0.22	0.15
0.1	3	5	2	1.98	0.80	0.00	1.01	0.00
0.01	3	2	2	3.63	1.40	0.00	1.00	0.00
0.005	3	2	2	4.10	1.40	0.00	1.00	0.00
0.005	3	2	1	4.32	1.60	0.00	1.00	0.00
0.2	3	2	2	2.76	1.00	0.11	0.89	0.00
0.15	3	2	2	1.82	0.80	0.00	1.00	0.00
0.05	3	5	2	1.90	0.80	-0.07	1.00	0.00

The model demonstrates that as average particle size increases, the imogolite proportion also increases, and that the inverse is true for the median particle size. The hydrolysis ratio constant was calculated to > 99.99% confidence, the elemental ratio constant was calculated to 99% confidence, and the concentration and mean radius size

constants were calculated to >98% confidence. The p-value for the entire model is 9×10^{-14} . The intercept of the model and the median particle size were found to be statistically insignificant with a p-value of 0.15 and 0.07 respectively. The rate of NaOH addition was found to decrease the overall confidence of the model, with a p-value that suggested addition rate did not influence endmember proportion, and so was omitted. The adjusted R^2 of the model is 0.98. The RMSE of the model is 0.05, meaning that the model can predict the imogolite proportion to within $\pm 5\%$.

The three overlapping factors for both equations 1 and 4 (concentration Al:Si ratio, OH:Al ratio) shared identical direction, and the coefficients were all within a standard error of one another. The similarity of the models is described well by the residuals of the data shown in Figure 7. The DW statistic for equation 4 was 1.84, which failed to reject the null hypothesis at 99% confidence. Visually, there does appear to be a linear trend in the residuals at lower proportions of imogolite, with both models.

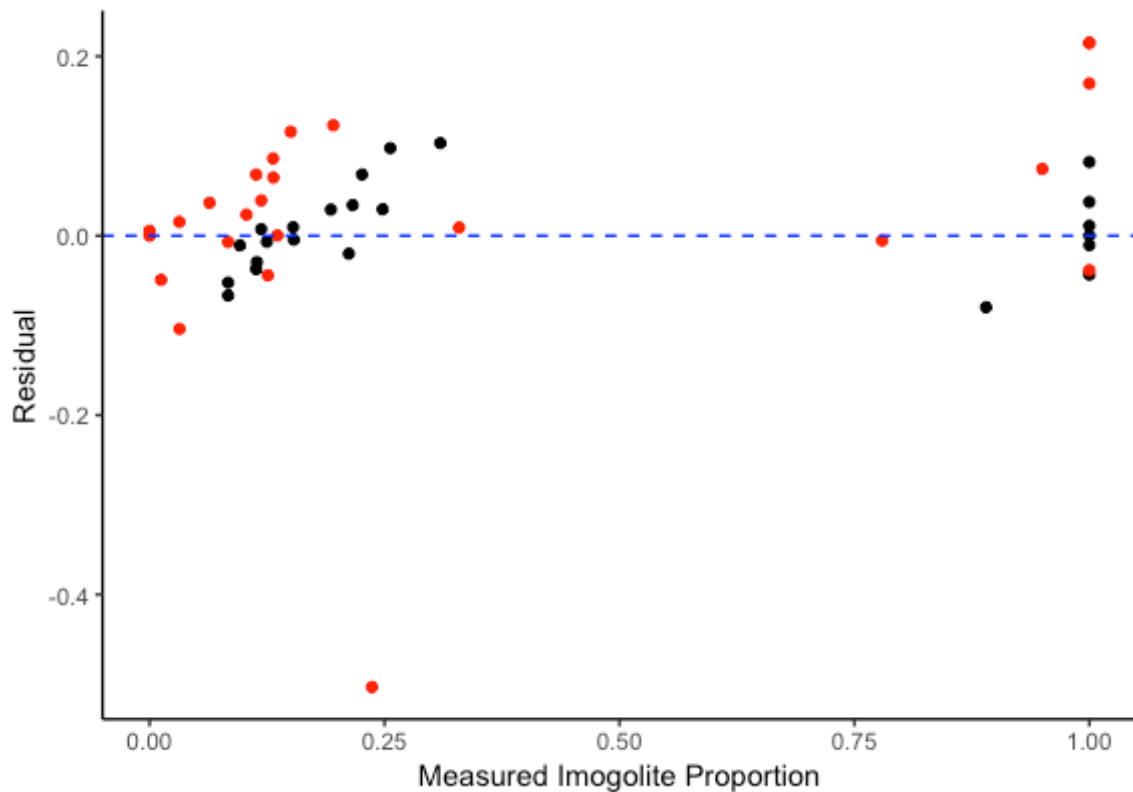


Figure 7

Residuals of the imogolite proportion models for the data without (red) and with (black) particle size data collected.

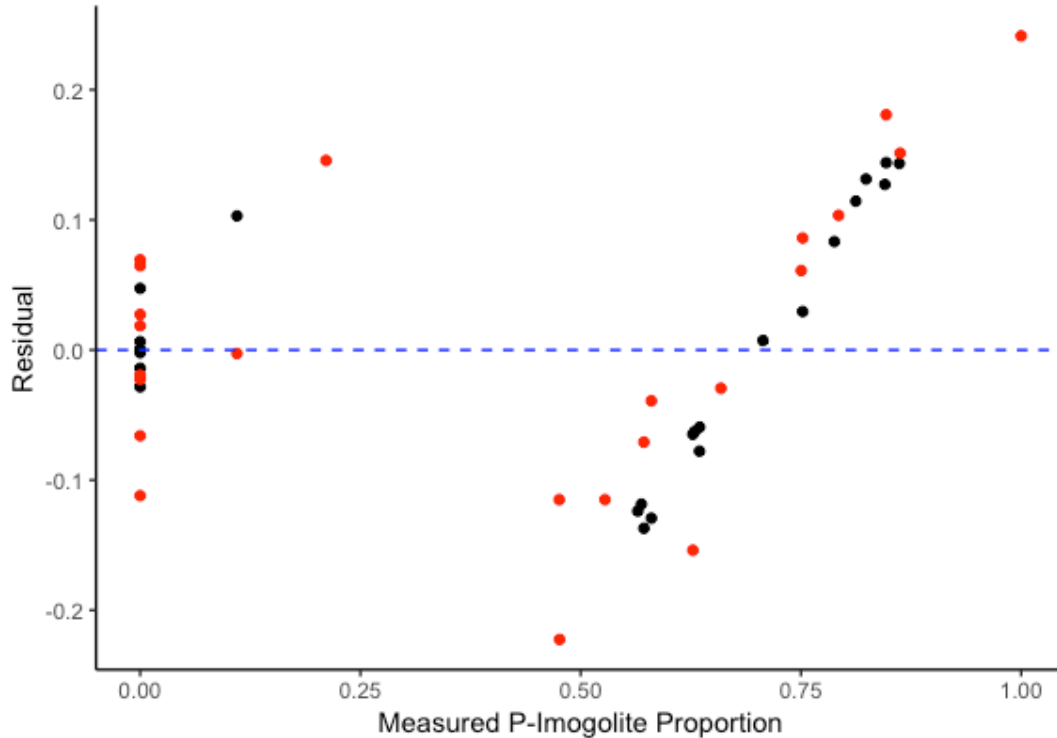


Figure 8

Residuals of the proto-imogolite proportion models for the data without (red) and with (black) particle size data collected.

The proto-imogolite proportion of this second data set was modeled by:
 $PI = 1.08 - 0.34hydro + 0.37C - 0.0007Al : Si - 0.034R_{avg} + 0.050R_{med}$ [Eq. 5].

This model shares the same trends as the model developed through the data in Table 1, and the absolute factors are within a standard deviation. The model describes relationships that are opposite those of the imogolite proportion, including the particle size where mean particle size growth leads to less proto-imogolite.

The p-value of the overall model is 3×10^{-8} , along with an R^2 value of 0.91, indicating a high degree of confidence that the model is explaining 91% of the variance in the data. Unlike the imogolite proportion model, the individual variables are less significant than when combined into the general model. The coefficient for the intercept, hydrolysis, and concentration were significant to >95%, but the rest of the factors ranged from p-values of 0.1 to 0.8. The RMSE of this model is also higher than that of the imogolite model, at 0.09; this model can predict the proto-imogolite proportion, on average, to within 9%.

The DW statistic for the residuals of this model is 0.5, which confirms the alternative hypothesis that there is positive autocorrelation in the residuals. Visual interpretation of the residuals shown in figure 8 also shows both the similarity of the models and the linear, predictable trend at high concentrations of proto-imogolite.

4. Discussion

4.1 Growth stages of aluminosilicate nanoparticles

Results from prior studies conducted at similar condition suggest that Stage 1 involves the rapid nucleation and growth of gibbsite-like $\text{Al}(\text{OH})_3$ nanoparticles (Wada et al., 1979; Ohashi et al., 2002) (Figure 1) . Stage 2 is thought to involve silica attachment to the sheets resulting in the formation of the local imogolite structure (Du et al., 2018). This occurs through the oxolation mechanism where some of the $-\text{OH}$ groups on the gibbsite-like sheets are substituted by the silica tetrahedra, releasing 3 moles of H_3O^+ into solution per mole of Si attached. (Arancibia-Miranda et al., 2013). The stabilization in pH and particle nucleation and growth with time suggests that the development of the imogolite structure slows and eventually ceases during Stage 3.

4.2 Influence of synthesis conditions on phase abundance

The models developed in equations 1-5 describe the relationship between the system of physical and chemical conditions used for synthesis, and the abundances of imogolite, proto-imogolite, and amorphous silica the final synthesized products.

The hydrolysis ratio was determined to be the most important factor controlling morphology. As the hydrolysis ratio increased from 1 to 3, the proportion of imogolite increased, and the proportion of proto-imogolite formed decreased. A consequence of increasing the hydrolysis ratio is that the initial pH of solution also increases. With a hydrolysis ratio of 1, the pH ranged from 3.3-4.2, while when the hydrolysis ratio was set to 3, the pH ranged from 9.2 to 10. Allophanes have been shown to be unstable in alkaline conditions, where defect pores develop, enlarge, and break down the structure (Wang et al., 2018). A similar mechanism would likely prevent proto-imogolites from forming in alkaline conditions, explaining the decrease of proto-imogolite proportion with increasing hydrolysis ratio.

Previous studies of imogolite synthesis have found that at hydrolysis ratios below 1.5, tubular structures were unable to form, and significant structural defects below 2.0 were observed (Levard et al., 2011b). The imogolite model supports that experimental result; a decreasing hydrolysis ratio resulted in significantly decreased imogolite proportion. Experimentally, the average imogolite portion of samples with a hydrolysis ratio below 1.5 was 9%, which agrees well with the previously reported findings.

The Al:Si ratio was also found to be a significant factor that influences final phase composition. As the relative abundance of Al increases, the imogolite proportion increases. The idealized formula for imogolite is $\text{Al}_2(\text{OH})_3\text{SiO}_3\text{OH}$, with a 2:1 Al:Si ratio. As the ratio is deviated from, and the Si increases, the amount of amorphous silica increases as well. This amorphous silica likely interferes with the growth kinetics of imogolite. Proto-imogolite particles have been shown to be able to incorporate silica

into its structure, polymerizing chains of Si branching off from the tetrahedral sites, creating a Si-rich local structure (Levard et al., 2012). This is reflected in the model equations, where as the relative amount of Si increases, the proto-imogolite proportion also increases.

The models show that increasing concentration of starting reagents leads to a lower proportion of imogolite. Based on reported literature results, producing high concentrations of nucleated particles have been suggested to impede imogolite growth kinetics, especially growing longer tube structures (Maillet et al., 2011).

Based on results from numerical modeling, it has been proposed that there is a size threshold at 4 nm for precursor particles where the energetically favorable morphology for growth transitions from spherical to tubular (Thill et al., 2017). This result agrees with the *in situ* studies that are described by equations 4 and 5. The precursor particles that were >3.6 nm in diameter had, on average, an increase of imogolite final phase composition of 0.92. This confirms the result of the numerical modeling experimentally, with a slight adjustment to the morphological transition to 3.6nm.

4.3 Evidence of allophane versus proto-imogolite production in the literature

Extensive syntheses of nanosized aluminosilicates have been carried out by a variety of researchers at differing starting conditions. Many of these starting conditions overlap directly with those chosen for this study. Although the authors of this study never produced any well-formed nanospheres 3-5 nm sizes that were expected based on what has been described previously for allophane, multiple other studies utilizing similar methods and conditions report allophane production. The XRD patterns of allophane and proto-imogolite are indistinguishable, and so cannot be used as evidence towards the production of allophane (Levard et al., 2012). HRTEM images are the strongest evidence for allophane as a direct measure of morphology, but it is not a ubiquitous technique used, when distinguishing between imogolite and allophane. Recent models of allophanic products call into question the idealized 3-5nm spherical structures; because it has a variable Al:Si ratio and the structure is not as well defined (Yuan et al., 2016). It has been proposed that allophane, because of its variable composition, should be thought of as a series of minerals rather than a single species (Parfitt and Kimble, 1989). It is the opinion of the authors that often what is called allophane in the literature, unless is clearly demonstrated through TEM imagery, is actually proto-imogolite in a variety of morphologies.

4.4 Modeled versus experimental pXRD patterns produced in literature

The generalizability of the model was tested by comparing the model's prediction of phase abundance and the reported pXRD pattern, based on given starting conditions. Whether or not the researchers describe the products as

allophane or proto-imogolite, the result should be the same because they share indistinguishable XRD patterns. The key differential is between those and imogolite, which has longer range order and a distinct pXRD pattern. Synthesis conditions reported in literature were run by the models, resulting in predicted phase abundances of imogolite, proto-imogolite, and amorphous silica. Using this result, an expected pXRD pattern, based on the conditions, was produced. This was then compared to the reported pXRD pattern in the study where those conditions were used (Figure 9)..

Ohashi et al. (2002) were attempting to synthesize allophane from high concentration solutions, using starting concentrations of 0.1M, a Si:Al ratio of 0.75, and did not use NaOH to induce hydrolysis. Despite using conditions beyond the scope used to develop the model, as well as a slightly different silica reagent (Na_4SiO_4) there is still strong agreement between the patterns.

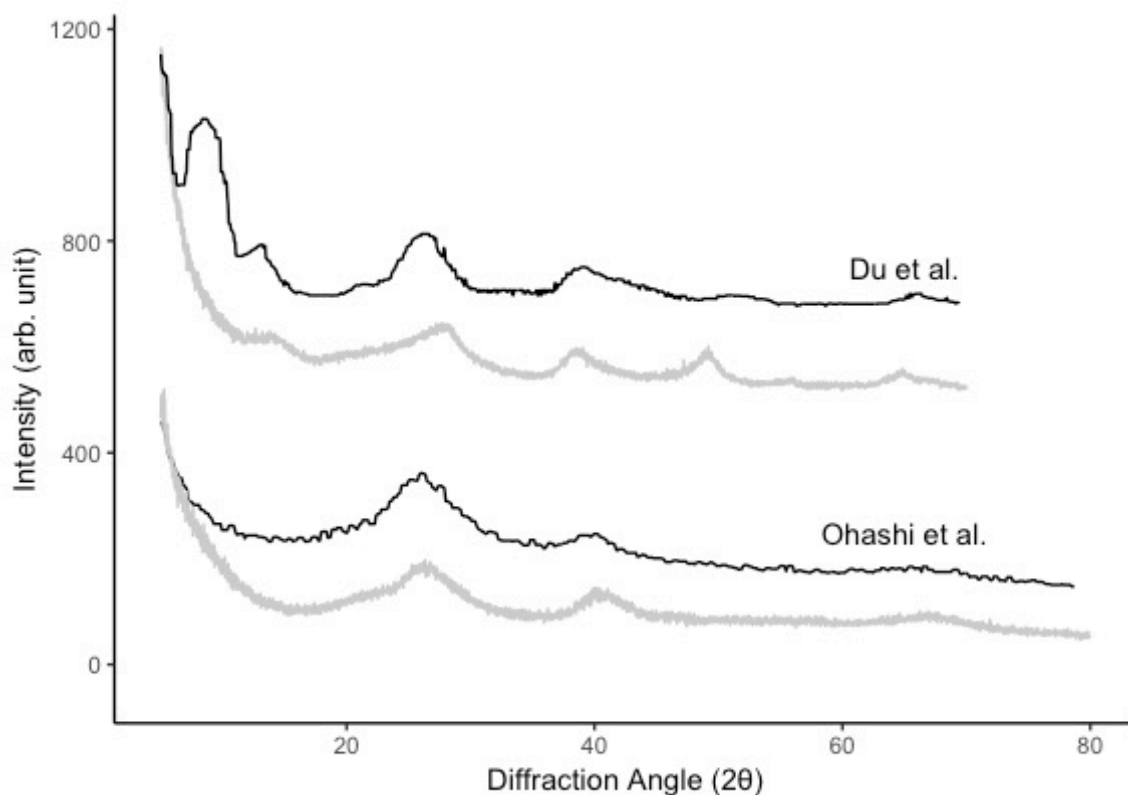


Figure 9

Experimental XRD pattern of the Ohashi et al. reported synthetic allophane, and the Du et al. reported synthetic imogolite. The experimentally derived patterns are in black, and the modeled patterns based on the given starting conditions are in grey.

Du et al. (2017) investigated the effects of heating time on imogolite formation. The results of the final product heated for 5 days closely aligns with the modeled result shown in Figure 9. The model correctly predicts the resulting product to be primarily imogolite, and aligns with the experimental pattern. There is a missing peak in the model at 0.94 nm that is likely due to a higher degree of ordering of the imogolite tubes in the sample that Du et al. produced. The starting conditions that Du et al. used were

starting reagent concentrations of 0.15M AlCl_3 , 0.1M Na_4SiO_4 , and added NaOH to reach a pH of 5.5. Once again, using conditions not explicitly tested in developing the model, there is still good agreement between what the models expect to result from the conditions, and the reported experimental pattern.

These examples demonstrate how the ability of our model to predict the outcome of the reported syntheses from literature review, even when synthesis conditions outside the bounds used to produce the model were used. This confirms that the model is more widely applicable than the specific synthesis method and products produced in this study, and can provide valuable information to researchers working with nanosized aluminosilicates.

4.5 The significance of the in situ data

Based on the conclusion of the previous section, the importance of studying these systems *in situ* is apparent. The addition of the *in situ* size data resulted in the models improving from explaining 86 and 88% of the variance, to 91 and 98%, respectively. These complex synthesis systems cannot be fully understood when all the analysis is performed after the formation of the particles. Critical information about formation conditions and parameters comes from the formation process itself. The SAXS results also demonstrated some more generalized principals of particle growth and nucleation that may be applicable to other geochemical systems.

4.6 Multivariate approach to explaining geochemical systems

Along with utilizing *in situ* data, a multivariate regression approach has allowed for the description for the system as a whole. Using this systematic methodology creates the opportunity to explore unaddressed questions. Modeling predicts that imogolite is energetically favored to form when precursor particles are larger than 4nm, but it has also been shown experimentally to be unable to form when the hydrolysis ratio is under 1.5. Using this multivariate approach, assuming correct quantification and explanation for the factors influencing the system, we can ask a question such as, what would be expected to develop if precursor particles were large, but were forming at low hydrolysis ratios? Assuming a starting condition similar to other literature studies, and given a standard particle size of 4nm, which has been found repeatedly during *in situ* investigations, the model would suggest that even with a large particle size, imogolite would be mostly unable to form at low hydrolysis conditions. Conversely, given a similar system but with a high hydrolysis ratio and small particles, where proto-imogolites have been found to be structurally unstable, but also should be energetically favorable, the model predicts that minimal proto-imogolite will form. This leads to the conclusion that the hydrolysis ratio is a stronger control on the system than the particle size, which may give insights into the formation process, and reveals the strength of this systems approach.

5. Conclusions

We used a systematic synthesis procedure combined with a suite of complementary analytical techniques, assessed using linear combination fitting and analyzed with multivariate regression techniques to determine the influence of starting physical and chemical conditions on the final phase composition of nanosized aluminosilicate products. Although synthesis methods previously reported to have formed allophane were used, the only definite products produced were imogolite and proto-imogolite. Using a systems approach allowed us to examine how concentration of starting reagents, elemental ratios, hydrolysis ratios, and precursor particle sizes all simultaneously and independently influenced the proportion of each endmember. We produced linear models with statistically significant high predictive power that quantitatively described the effect each factor had on the phase abundance of each endmember. Two different data sets produced linear models with similar coefficients and identical conclusions about the direction each parameter drove the system. The models accurately represented what was found experimentally in several literature studies.

These models can help answer questions about nanoparticle formation, and address factors in a uniquely systems-based approach not yet employed in this field. This approach can be applied to a multitude of geochemical systems to produce predictive models about crystallization. Using these models we can probe questions about what chemical and physical properties are most important during mineral or precursor formation, which can lead to insights about mechanisms and reactions.

Works Cited

- Abidin, Z., Matsue, N., and Henmi, T., 2007, Nanometer-scale chemical modification of nano-ball allophane: *Clays and Clay Minerals*, v. 55, p. 443–449, doi: 10.1346/CCMN.2007.0550410.
- Arai, Y., Sparks, D.L., and Davis, J.A., 2005, Arsenate adsorption mechanisms at the allophane - Water interface: *Environmental Science and Technology*, v. 39, p. 2537–2544, doi: 10.1021/es0486770.
- Arancibia-miranda, N., Escudey, M., Molina, M., and García-gonzález, M.T., 2013, Kinetic and Surface Study of Single-Walled Aluminosilicate Nanotubes and Their Precursors: , p. 126–140, doi: 10.3390/nano3010126.
- Du, P., Yuan, P., Liu, D., Wang, S., Song, H., and Guo, H., 2018, Calcination-induced changes in structure, morphology, and porosity of allophane: *Applied Clay Science*, v. 158, p. 211–218, doi: 10.1016/J.CLAY.2018.03.035.
- Du, P., Yuan, P., Thill, A., Annabi-Bergaya, F., Liu, D., and Wang, S., 2017, Insights into the formation mechanism of imogolite from a full-range observation of its sol-gel growth: *Applied Clay Science*, v. 150, p. 115–124, doi: 10.1016/j.clay.2017.09.021.
- González, R.I., Ramírez, R., Rogan, J., Valdivia, J.A., Munoz, F., Valencia, F., Ramírez, M., and Kiwi, M., 2014, Model for self-rolling of an aluminosilicate sheet into a single-walled imogolite nanotube: *Journal of Physical Chemistry C*, v. 118, p. 28227–28233, doi: 10.1021/jp508637q.
- Gustafsson, J.P., 2001, The surface chemistry of imogolite: *Clays and Clay Minerals*, v. 49, p. 73–80, doi: 10.1346/CCMN.2001.0490106.
- Harsh, J., 2002, Chapter 9 Allophane and Imogolite: , p. 291–322.
- Harsh, J.B., Traina, S.J., Boyle, J., and Yang, Y., 1992, ADSORPTION OF CATIONS ON IMOGOLITE AND THEIR EFFECT ON SURFACE CHARGE CHARACTERISTICS 1 *Materials synthesis*: v. 40, p. 700–706.
- Huang, Y.T., Lowe, D.J., Churchman, G.J., Schipper, L.A., Cursons, R., Zhang, H., Chen, T.Y., and Cooper, A., 2016, DNA adsorption by nanocrystalline allophane spherules and nanoaggregates, and implications for carbon sequestration in Andisols: *Applied Clay Science*, v. 120, p. 40–50, doi: 10.1016/j.clay.2015.11.009.
- Iyoda, F., Hayashi, S., Arakawa, S., Okamoto, M., and Hayashi, H., 2014, Synthesis and adsorption characteristics of hollow spherical allophane nano-particles: *AIP Conference Proceedings*, v. 1593, p. 244–247, doi: 10.1063/1.4873773.
- Levard, C., Doelsch, E., Basile-Doelsch, I., Abidin, Z., Miche, H., Masion, A., Rose, J., Borschneck, D., and Bottero, J.Y., 2012, Structure and distribution of allophanes, imogolite and proto-imogolite in volcanic soils: *Geoderma*, v. 183–184, p. 100–108, doi: 10.1016/j.geoderma.2012.03.015.
- Levard, C., Masion, A., Rose, J., Doelsch, E., Borschneck, D., Olivi, L., Chaurand, P., Dominici, C., Ziarelli, F., Thill, A., Maillat, P., and Bottero, J.Y., 2011a, Synthesis of Ge-imogolite : influence of the hydrolysis ratio on the structure of the nanotubes: *Phys. Chem. Chem. Phys.*, v. 13, p. 14516–14522, doi: 10.1039/c1cp20346k.
- Levard, C., Masion, A., Rose, J., Doelsch, E., Borschneck, D., Olivi, L., Chaurand, P.,

- Dominici, C., Ziarelli, F., Thill, A., Maillet, P., and Bottero, J.Y., 2011b, Synthesis of Ge-imogolite : influence of the hydrolysis ratio on the structure of the nanotubes: , p. 14516–14522, doi: 10.1039/c1cp20346k.
- Levard, C., Rose, J., Thill, A., Masion, A., Doelsch, E., Maillet, P., Spalla, O., Olivi, L., Cognigni, A., Ziarelli, F., and Bottero, J.Y., 2010, Formation and growth mechanisms of imogolite-like aluminogermanate nanotubes: *Chemistry of Materials*, v. 22, p. 2466–2473, doi: 10.1021/cm902883p.
- Maillet, P., Levard, C., Spalla, O., Masion, A., Rose, J., and Thill, A., 2011, Growth kinetic of single and double-walled aluminogermanate imogolite-like nanotubes: an experimental and modeling approach: *Phys. Chem. Chem. Phys.*, v. 13, p. 2682–2689, doi: 10.1039/C0CP01851A.
- Mansouri, E., Feizi, F., Jafari Rad, A., and Arian, M., 2018, Remote-sensing data processing with the multivariate regression analysis method for iron mineral resource potential mapping: A case study in the Sarvian area, central Iran: *Solid Earth*, v. 9, p. 373–384, doi: 10.5194/se-9-373-2018.
- Montarges-Pelletier, E., Bogenez, S., Pelletier, M., Razafitianamaharavo, A., Ghanbaja, J., Lartiges, B., and Michot, L., 2005, Synthetic allophane-like particles: Textural properties: *Colloids and Surfaces A: Physicochemical and Engineering Aspects*, v. 255, p. 1–10, doi: 10.1016/j.colsurfa.2004.11.036.
- Musić, S., Filipović-Vinceković, N., and Sekovanić, L., 2011, Precipitation of amorphous SiO₂ particles and their properties: *Brazilian Journal of Chemical Engineering*, v. 28, p. 89–94, doi: 10.1590/S0104-66322011000100011.
- Ohashi, F., Wada, S.-I., Suzuki, M., Maeda, M., and Tomura, S., 2002, Synthetic allophane from high-concentration solutions: nanoengineering of the porous solid: *Clay Minerals*, v. 37, p. 451–456, doi: 10.1180/0009855023730052.
- Paineau, E., Paineau, and Erwan, 2018, Imogolite Nanotubes: A Flexible Nanoplatform with Multipurpose Applications: *Applied Sciences*, v. 8, p. 1921, doi: 10.3390/app8101921.
- Parfitt, R.L., 2009, Allophane and imogolite: role in soil biogeochemical processes: *Clay Minerals*, v. 44, p. 135–155, doi: 10.1180/claymin.2009.044.1.135.
- Parfitt, R.L., and Kimble, J.M., 1989, Conditions for Formation of Allophane in Soils: *Soil Science Society of America Journal*, v. 53, p. 971–977, doi: 10.2136/sssaj1989.03615995005300030057x.
- Sharp, T.G., and Chang, S.L.Y., 2017, High Resolution Imaging of Short-Range Order Materials (Allophane) with Aberration Corrected TEM and Direct Electron Detection: *Microscopy and Microanalysis*, v. 23, p. 2152–2153, doi: 10.1017/S1431927617011424.
- Thill, A., 2016, From Molecular Precursor to Imogolite Nanotubes, *in* *Developments in Clay Science*, v. 7, doi: 10.1016/B978-0-08-100293-3.00018-2.
- Thill, A., Picot, P., and Belloni, L., 2017, A mechanism for the sphere/tube shape transition of nanoparticles with an imogolite local structure (imogolite and allophane): *Applied Clay Science*, v. 141, p. 308–315, doi: 10.1016/j.clay.2017.03.011.
- WADA, S. -I, ETO, A., and WADA, K., 1979, Synthetic Allophane and Imogolite: *Journal of*

Soil Science, v. 30, p. 347–355, doi: 10.1111/j.1365-2389.1979.tb00991.x.
Wang, S., Du, P., Yuan, P., Zhong, X., Liu, Y., and Liu, D., 2018, Applied Clay Science
Changes in the structure and porosity of hollow spherical allophane under alkaline
conditions: Applied Clay Science, v. 166, p. 242–249, doi:
10.1016/j.clay.2018.09.028.